Symmetry and Rigidity for Boosting Erbium-Based Molecular Light-Upconversion in Solution

Soroush Naseri, Inès Taarit, Hélène Bolvin, Jean-claude Bünzli, Alexandre Fürstenberg, Laure Guénée, Giau Le-Hoang, Mohsen Mirzakhani, Homayoun Nozary, Arnulf Rosspeintner, et al.

Symmetry and Rigidity for Boosting Erbium-Based Molecular Light-Upconversion in Solution.

Soroush Naseri,[*a] *Inès Taarit,*[*a] *Hélène Bolvin,*[d] *Jean-Claude Bünzli,*[e] *Alexandre Fürstenberg,*[a],[c] *Laure Guénée,*[b] *Giau Le-Hoang,*[a] *Mohsen Mirzakhani,*[a] *Homayoun Nozary,*[a] *Arnulf Rosspeintner,*[c] *Claude Piguet*[*a]

[a] Dr S. Naseri, Dr I. Taarit, Dr A. Fürstenberg, Dr G. Le-Hoang, Dr M. Mirzakhani, Dr H. Nozary, Prof. Dr C. Piguet
Department of Inorganic and Analytical Chemistry, University of Geneva, 30 quai E. Ansermet, CH-1211 Geneva 4, Switzerland.
Email: Soroush.Naseri@unige.ch; Ines.Taarit@unige.ch; Claude.Piguet@unige.ch

[b] Dr L. Guénée
Laboratory of Crystallography, University of Geneva, 24 quai E. Ansermet, CH-1211 Geneva 4, Switzerland.

[c] Dr A. Rosspeintner, Dr A. Fürstenberg
Department of Physical Chemistry, University of Geneva, 30 quai E. Ansermet, CH-1211 Geneva 4, Switzerland.

[d] Dr H. Bolvin
Laboratoire de Chimie et Physique Quantiques, CNRS, Université Toulouse III, 118 route de Narbonne, F-31062 Toulouse, France.

[e] Prof. Dr. J.-C. Bünzli
Institute of Chemical Sciences & Engineering, Swiss Federal Institute of Technology (EPFL), Lausanne, Switzerland.

Supporting information for this article is available at WWW under
hhhps://doi.org/10.1002/chem.xxxxx.

Abstract

Previously limited to highly symmetrical homoleptic triple-helical complexes $[Er(\mathbf{Lk})_3]^{3+}$*, where* **Lk** *are polyaromatic tridentate ligands, single-center molecular-based upconversion using linear optics and exploiting the excited-state absorption mechanism (ESA) greatly benefits from the design of stable and low-symmetrical* $[\mathbf{Lk}Er(hfa)_3]$ *heteroleptic adducts* (hfa^- *= hexafluoroacetylacetonate anion). Depending on (i) the extended* π*-electron delocalization, (ii) the flexibility, and (iii) the heavy atom effect brought by the bound ligand* **Lk***, the near-infrared (801 nm) to visible green (542 nm) upconversion quantum yield measured for* $[\mathbf{Lk}Er(hfa)_3]$ *in solution at room temperature can be boosted by up to three orders of magnitude.*

Introduction

The conversion of low-energy photons toward higher energies, much beyond the standard thermally-activated vibrational Stokes' shifts, is referred to as light upconversion. It remains challenging in both physics and chemistry since it suggests some apparent deviations from the well-accepted law of energy degradation.[1] Such process was theoretically predicted by Goeppert-Mayer in 1931[2] when considering the consequences of the non-linear dependence of the refractive index on incident light.[3],[4] Indeed, the polarization of the macroscopic medium produced by an intense electric field at ω frequency results in a linear response at the same frequency (= linear optics), together with additional oscillating polarizations of the medium at twice (2ω, second order polarization) and thrice (3ω, third order polarization) the incident frequency (= non-linear optics, NLO).[1] A related approach applies for molecules characterized by linear α polarizability (linear response), together with first β and second γ hyperpolarizabilities (non-linear response at higher frequencies).[1] However, even for modern optimized polarized materials,[5],[6] the non-linear responses are so weak (typically $\beta/\alpha = 10^{-8}$

for first-order and $\gamma/\alpha = 10^{-12}$ for second-order hyperpolarizabilities) that NLO upconversion had to wait the discovery of intense coherent laser excitation beams in the early sixties[7] to be experimentally demonstrated.[8],[9] Nowadays, the easy access to intense pulsed-femtosecond lasers (incident power intensity $P \approx 10^9$ W·cm^{-2}) may compensate for the inherent inefficiency of NLO materials, leading to modern applications as deeply penetrating beams for addressing biological probes[10]-[13] or as optical limiting devices.[14]-[16]

a)

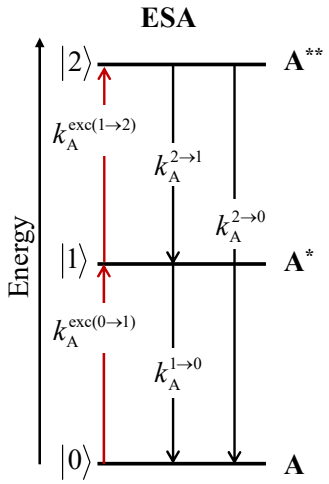

b)

$$\begin{pmatrix} dN_A^{|0\rangle}/dt \\ dN_A^{|1\rangle}/dt \\ dN_A^{|2\rangle}/dt \end{pmatrix} = \begin{pmatrix} -k_A^{exc(0\to1)} & k_A^{1\to0} & k_A^{2\to0} \\ k_A^{exc(0\to1)} & -\left(k_A^{exc(1\to2)} + k_A^{1\to0}\right) & k_A^{2\to1} \\ 0 & k_A^{exc(1\to2)} & -\left(k_A^{2\to1} + k_A^{2\to0}\right) \end{pmatrix} \times \begin{pmatrix} N_A^{|0\rangle} \\ N_A^{|1\rangle} \\ N_A^{|2\rangle} \end{pmatrix}$$

Scheme 1. a) Kinetic scheme and b) associated differential matrix equations depicting the modeling of the one-ion excited-state absorption (ESA) process occurring upon off-resonance irradiation into the activator-centered absorption band where $k_A^{exc(i\to j)}$ (in s^{-1}) corresponds to the excitation rate constants (eq 1)[57] and $k_A^{j\to i}$ stands for the global (sum of radiative and non-radiative contribution) decay rate constant of level j into level i.[18]

With this in mind, detectable light-upconversion induced under weak excitation power intensities compatible with normal lamps or solar irradiance ($P \approx 0.1$-1.0 W·cm^{-2}) is limited to the exclusive use of linear optics (Scheme 1a).[17] An initial photon absorption reaches a real intermediate excited state with a long lifetime (A* in Scheme 1), which is exploited as a relay

for the absorption of a second photon leading to a higher excited state A^{**}. An ultimate radiative relaxation to the ground state A, as quantified by its intrinsic radiative quantum yield $\phi_A = k_{A,rad}^{2\rightarrow 0} \Big/ \left(k_A^{2\rightarrow 1} + k_A^{2\rightarrow 0} \right)$, completes the light-upconversion process (Scheme 1).[17] A first hint based on successive absorptions relying on linear optics was proposed by Bloembergen for the potential design of infra-red quantum counters.[19] For addressing this challenge, chemists logically focused on systems possessing long-lived intermediate excited states, *i.e.*, triplet states in polyaromatic organic molecules[20],[21] or $^{2S+1}L_J$ spectroscopic levels in f-block trivalent centers doped in low-phonon ionic solids.[22],[23] Due to the strict respect of the spin selection rule in polyaromatic scaffolds (negligible spin-orbit coupling), there is no chance to reach a strongly emissive singlet state via the absorption of a second photon by an intermediate long-lived triplet excited state in pure organic chromophores (ESA mechanism). Consequently, organic-based (linear) upconversion exploits the alternative triplet-triplet annihilation mechanism (TTA), which requires the diffusion and collision of two excited aromatic triplet acceptors.[24]-[26] This methodology is thus mainly[27] limited to intermolecular processes occurring in solution, rubbery polymeric materials, or solid matrices.[28],[29],[30] This constraint is removed for 4f-block elements since their considerable spin-orbit coupling constants relax the spin rule. However, the lanthanide-based excited-state absorption (ESA) upconversion mechanism remains limited by the weak absorption coefficients accompanying the parity-forbidden forced electric dipole transitions ($k_A^{exc(i\rightarrow j)}$ in Scheme 1). A clever bypass, referred to as Energy Transfer Upconversion: ETU, considers the use of additional strongly absorbing sensitizers (S) as partners for feeding the lanthanide activator (A) via successive S→A energy transfers.[17],[23],[31],[32] Using plasmon surfaces[29],[33]-[35] or organic dyes[29],[36],[37] as sensitizers for lanthanide activators in doped ionic solids or nanoparticles opened the door toward applications[29] with upconversion quantum yields overpassing 10% and large associated brightness.[38]-[40]

Miniaturization to reach the molecular level in lanthanide coordination complexes is hindered by the drastic reduction of the lifetimes of the intermediate excited relays ($\tau_{\mathrm{A}}^{|1\rangle} = 1/k_{\mathrm{A}}^{1\rightarrow 0}$ in Scheme 1) due to a massive increase in non-radiative relaxation processes produced by the considerable thermal vibrational bath found in molecules.[41] Consequently, the few dozens of lanthanide-containing molecular complexes displaying detectable (linear) light upconversion under weak excitation intensity powers ($P \leq 40$ W·cm^{-2})[18],[42]-[49] relied mainly on ETU[50]-[53] or on related multicenter cooperative upconversion (CU) processes.[54]-[56] However, the synthetic difficulties associated with the non-statistical combination of sensitizers and activators within a single molecular entity for programming ETU or CU mechanisms, particularly when both partners are open-shell labile lanthanide cations,[48],[54]-[56] pave the way for the single-center excited-state absorption mechanism (ESA) to rise as the ultimate fully controlled upconversion process programmed at the molecular level in the absence of statistical doping.[57]-[60]

For boosting the ESA mechanism, the first criterion concerns the f-f absorption cross sections $\sigma_{\mathrm{A}}^{i\rightarrow j}$, which should be rationally programmed in the target coordination complexes to maximize the excitation rate constants $k_{\mathrm{A}}^{\mathrm{exc}(i\rightarrow j)}$ under reasonable pump intensities P (in W·cm^{-2}) as modeled in eq (1).[61]

$$k_{\mathrm{A}}^{\mathrm{exc}(i\rightarrow j)} = \frac{\lambda_{\mathrm{P}}}{hc} P\sigma_{\mathrm{A}}^{i\rightarrow j} = 3.8\cdot 10^{-21}\frac{\lambda_{\mathrm{P}}}{hc} P\varepsilon_{\mathrm{A}}^{i\rightarrow j} \qquad (1)$$

λ_{p} is the pump wavelength (in cm), h is the Planck constant (in J·s), and c is the speed of light in vacuum (in cm·s^{-1}). The absorption cross section of the activator $\sigma_{\mathrm{A}}^{i\rightarrow j}$ (in cm^2) is related to its decadic molar absorption coefficient $\varepsilon^{i\rightarrow j}$ (in L/mol·cm) with $\sigma^{i\rightarrow j} = 3.8\cdot 10^{-21}\varepsilon^{i\rightarrow j}$.[62]

Solving the differential matrix equation pertinent to the single-center ESA mechanism (Scheme 1b) for the steady-state (S-S) conditions $\left[dN_{\mathrm{A,S\text{-}S}}^{|i\rangle}/dt\right] = 0$ obtained under continuous excitation

pumping allows the modeling of the steady-state population density $N_{\mathrm{A,S\text{-}S}}^{|i\rangle}$ (eqs S3-S5 in Scheme S1, SI) and of the total upconversion quantum yield $\Phi_{\mathrm{A}}^{\mathrm{up}}$ (eq 2, $k_{\mathrm{A,rad}}^{j\to i}$ is the radiative contribution to the relaxation decay rate constant).

$$\begin{aligned}\phi_{\mathrm{A}}^{\mathrm{up}} &= \frac{\text{Total emitted photons/time unit}}{\text{Total absorbed photons/time unit}} = \frac{k_{\mathrm{A,rad}}^{2\to 0} N_{\mathrm{A,S\text{-}S}}^{|2\rangle}}{k_{\mathrm{A}}^{\mathrm{exc}(0\to 1)} N_{\mathrm{A,S\text{-}S}}^{|0\rangle} + k_{\mathrm{A}}^{\mathrm{exc}(1\to 2)} N_{\mathrm{A,S\text{-}S}}^{|1\rangle}} \\ &= \frac{k_{\mathrm{A}}^{\mathrm{exc}(1\to 2)} k_{\mathrm{A,rad}}^{2\to 0}}{\left(k_{\mathrm{A}}^{\mathrm{exc}(1\to 2)} + k_{\mathrm{A}}^{1\to 0}\right)\left(k_{\mathrm{A}}^{2\to 1} + k_{\mathrm{A}}^{2\to 0}\right) + k_{\mathrm{A}}^{\mathrm{exc}(1\to 2)} k_{\mathrm{A}}^{2\to 0}} \\ &\approx \frac{k_{\mathrm{A}}^{\mathrm{exc}(1\to 2)}}{k_{\mathrm{A}}^{1\to 0}} \times \frac{k_{\mathrm{A,rad}}^{2\to 0}}{k_{\mathrm{A}}^{2\to 1} + k_{\mathrm{A}}^{2\to 0}} \approx \left(3.8\cdot 10^{-21} \frac{\lambda_{\mathrm{P}}}{hc} P \varepsilon_{\mathrm{A}}^{1\to 2}\right) \tau_{\mathrm{A}}^{|1\rangle} \times k_{\mathrm{A,rad}}^{2\to 0} \tau_{\mathrm{A}}^{|2\rangle} = \eta_{\mathrm{A,ESA}} \times \phi_{\mathrm{A}} \end{aligned} \quad (2)$$

Under weak incident excitation power used for inducing linear upconversion in molecular complexes (P = 0.1-40 W·cm^{-2}),[18],[42]-[59] the rate constants of the excitation processes ($k_{\mathrm{A}}^{\mathrm{exc}(i\to j)}$) are largely dominated by the relaxation rate constants ($k_{\mathrm{A}}^{j\to i}$), and a negligible number of molecules exist in the excited levels ($N_{\mathrm{A,S\text{-}S}}^{|0\rangle} \approx N^{\mathrm{tot}} = 1$). The total upconversion quantum yield thus reduces to $\phi_{\mathrm{A}}^{\mathrm{up}} \approx \left(k_{\mathrm{A}}^{\mathrm{exc}(1\to 2)} / k_{\mathrm{A}}^{1\to 0}\right) \times \phi_{\mathrm{A}}$, where $\tau_{\mathrm{A}}^{|1\rangle} = \left(1/k_{\mathrm{A}}^{1\to 0}\right)$ is the lifetime of the intermediate excited relay level $|1\rangle$ and ϕ_{A} corresponds to the intrinsic quantum yield of the final upconverted emissive level $|2\rangle$. In solution at room temperature, where lanthanide complexes exist as isolated molecular species, the ESA mechanism has been implemented mainly in erbium complexes[46]-[18],[60] possessing $^4I_{13/2}$ excited relay with microsecond lifetimes and intrinsic emission quantum yield $\phi_{\mathrm{Er}} \approx 10^{-5}$ for the emissive Er($^4S_{3/2}$) level (Figure 1).[59] Combined with the limited excitation rate constants $k_{\mathrm{A}}^{\mathrm{exc}(1\to 2)} \approx 10$ s^{-1} computed with eq (1) at P = 25 W·cm^{-2},[59] the upconverting quantum yields reported for the molecular Er-based ESA-mechanism only reach $10^{-11} \leq \Phi_{\mathrm{Er}}^{\mathrm{up}}(\mathrm{ESA}) \leq 10^{-9}$, with a maximum value of $\Phi_{\mathrm{Er}}^{\mathrm{up}}(\mathrm{ESA}) = 1.7(2)\ 10^{-9}$ for the homoleptic triple-stranded complex [Er(Et-bzimpy)$_3$]$^{3+}$ (Figure 1).[59]

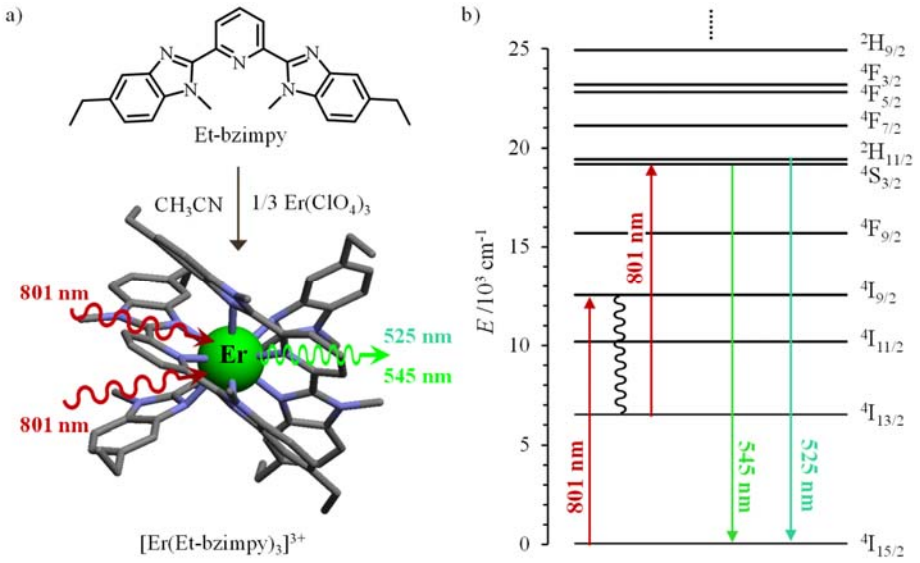

Figure 1. a) Synthesis and molecular structure of the triple-stranded helical $[Er(Et\text{-}bzimpy)_3]^{3+}$ complex (taken from the crystal structure of $[Er(Et\text{-}bzimpy)_3](ClO_4)_3 \cdot 2C_2H_3N$)[69] and b) proposed Excited-state Absorption (ESA) mechanism responsible for the red (801 nm)-to-green (520-540 nm) light upconversion observed in solution at room temperature.[59]

In our quest for pushing single-center molecular upconversion within acceptable efficiency limits, we hypothesized that lowering the symmetry around the Er(III) ion would lead to larger transition probabilities and, furthermore, rigidifying the ligands would lesser vibrational quenching. Subtle correlations exist between the intensities of the forced electric dipole 4f-4f transitions and the nature and geometry of the coordination spheres in lanthanide complexes due to the mixing between $4f^N$ states with opposite parity intra-metal excitation configurations (such as $4f^{N-1}5d$ or $4f^{N-1}5g$ following the Judd-Ofelt theory), or with intra-ligand excitation configurations via the crystal field generated by the oscillating induced dipole moments on the ligands following the dynamic coupling model.[63],[64] Being aware of these effects, we moved from highly symmetrical triple-helical $[Er\mathbf{L}_3]^{3+}$ complexes illustrated in Figure 1a[59] toward heteroleptic $[\mathbf{L}\boldsymbol{k}Er(hfa)_3]$ adducts based on the substituted tridentate 2,6-bis(benzimidazole)pyridine scaffolds (hfa^- = hexafluoroacetylacetonate).[65]-[68] The reported adducts are unique examples of fully characterized and stable heteroleptic lanthanide

complexes for which the single-center NIR to visible upconversion ESA mechanism is boosted by two to three orders of magnitude at room temperature in diluted solutions.

Results and discussion

Synthesis, structures and stabilities of the heteroleptic complexes [L*k*Er(hfa)$_3$] (L*k* = L1-L9).

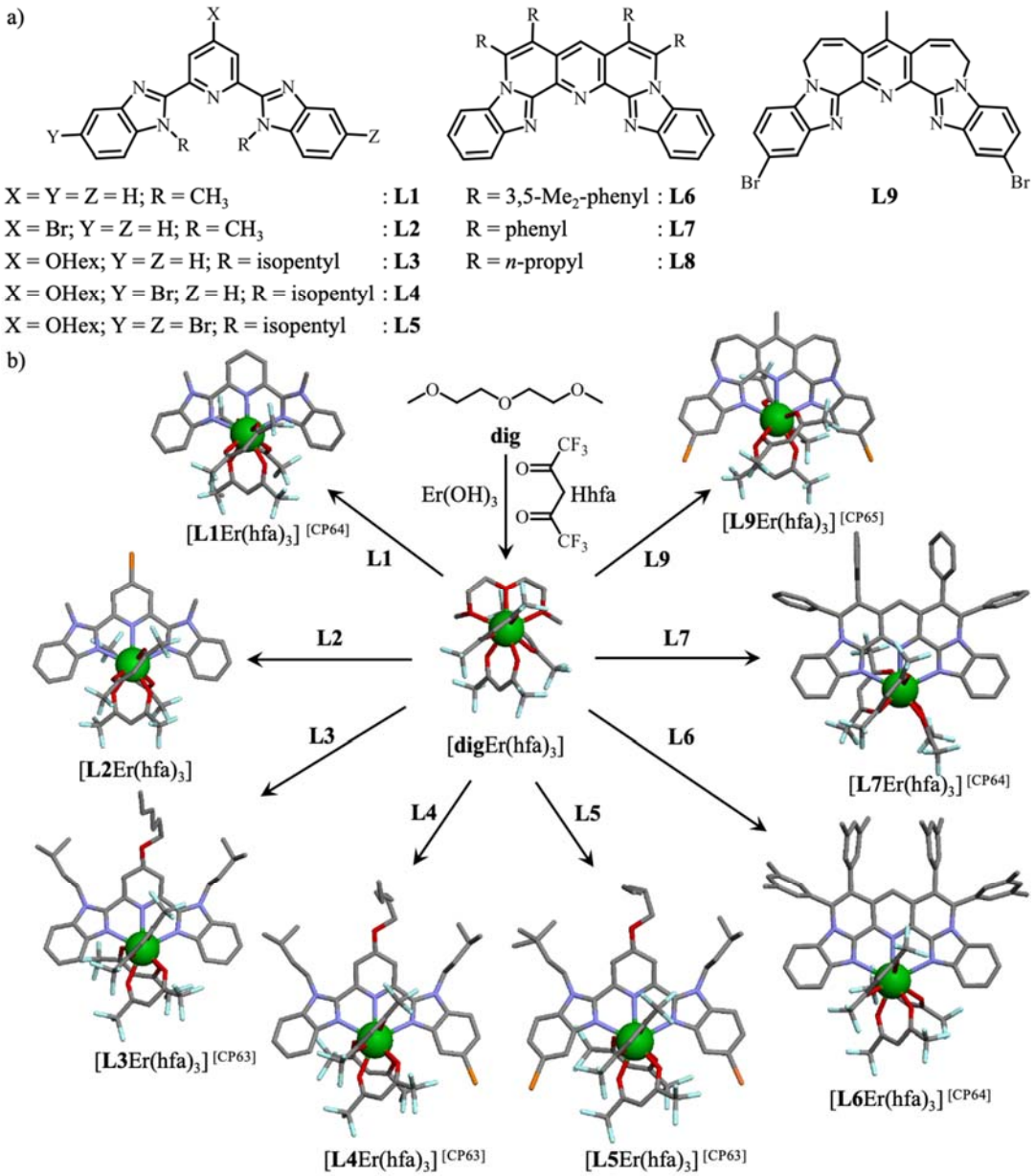

Figure 2. a) Polyaromatic tridentate receptors **L1**-**L9** used for hosting [Er(hfa)$_3$] units to give nine-coordinate [L*k*Er(hfa)$_3$] adducts. b) Synthesis and molecular structures of [L*k*Ln(hfa)$_3$] adducts (crystal structure: Ln = Er for **L1**, **L2**, **L7** and **L9**; Ln = Eu for **L3**-**L6**).[66]-[68]

The heteroleptic [**L*k***Er(hfa)$_3$] adducts (**L*k*** = **L1-L9**, Figure 2a) have been designed paying particular attention (i) to rationally introduce bromine substituents for exploring the heavy atom effect due to spin-orbit coupling (**L1**→**L2** and **L3**→**L4**→**L5**), (ii) to modulate rigidity and Ln-N bond distances while controlling the crystal-field effects and the magnitude of *J*-splitting (**L1**→**L6**-**L8**→**L9**)[59] and (iii) to extend the aromatic π-electron delocalization for lowering the energies of the ligand-based excited states and thus increasing dynamic coupling (**L1**-**L5** and **L9**→**L6**-**L8**).[64] All heteroleptic erbium [**L*k***Er(hfa)$_3$] complexes were obtained as stable mononuclear adducts (≥ 90% of the ligand speciation at 10^{-6} M, Table S1) from 1:1 host-guest reactions between **L*k*** and [**dig**Er(hfa)$_3$][65] (Tables S1-S2, Figure S1) conducted in dichloromethane.[66]-[68] The molecular structures for [**L*k***Er(hfa)$_3$], taken from the associated published crystal structures[66]-[68] together with the complementary data collected for [**L2**Er(hfa)$_3$] (Tables S3-S5, Figure S2), are gathered in Figure 2b. They show low-symmetry nine-coordinate [LnN$_3$O$_6$] coordination spheres that evolve from muffins for ligands **L3**-**L6** toward spherical capped square antiprisms for **L1**-**L2** and **L9** (Figure S3 and Table S6). In the solid state, the most compact, rigid, and preorganized adduct [**L7**Er(hfa)$_3$] is unique for approaching the spherical tricapped trigonal prism geometry, previously found for the triple-stranded [Er(Et-bzimpy)$_3$]$^{3+}$ complex and its analogues.[59] It is worth stressing here that the idealized D_{3h} symmetry, approached by the latter [ErN$_9$] coordination sphere in [Er(Et-bzimpy)$_3$]$^{3+}$, is automatically reduced to idealized C_{2v} for the [ErN$_3$O$_6$] unit in [**L7**Er(hfa)$_3$] because of the heteroleptic nature of the adduct possessing N and O donor groups.

The pertinent $\nu_{Ln\text{-}N}$ and $\nu_{Ln\text{-}O}$ bond valences[70] computed for the Er-N and Er-O bond lengths in the crystal structures of [**L*k***Er(hfa)$_3$] (eq A1-2 in Appendix 1, Tables S7-S9, Figure S4) show similar Ln-N$_{bzim}$ and Ln-O bond strengths, which are indeed larger than Ln-N$_{py}$ when the flexible ligands **L1**-**L5** and **L9** are bound to Ln(III) (Figures 3 and S4). The situation is reversed for the rigid polyaromatic ligands **L6**-**L7**, where the drop of $\nu_{Ln\text{-}Nbzim}$ observed in the associated

[**L*k***Ln(hfa)$_3$] adducts implies an unfavorable match between the preorganized ligand cavity and the entering [Ln(hfa)$_3$] metal container. Finally, to further highlight the unusual design of **L7**, one should realize that it is the only ligand of the series that does not possess alkyl groups (CH_2 or CH_3). This limits the contribution of high-energy vibrations to some weak C-H$_{arom}$ stretching bands around 3030 cm^{-1} in the IR spectrum (Figure S5). For all other ligands, the weak C-H$_{arom}$ stretching bands are completed with broader and more intense C-H$_{aliph}$ stretching bands covering the 2800-2950 cm^{-1} range.

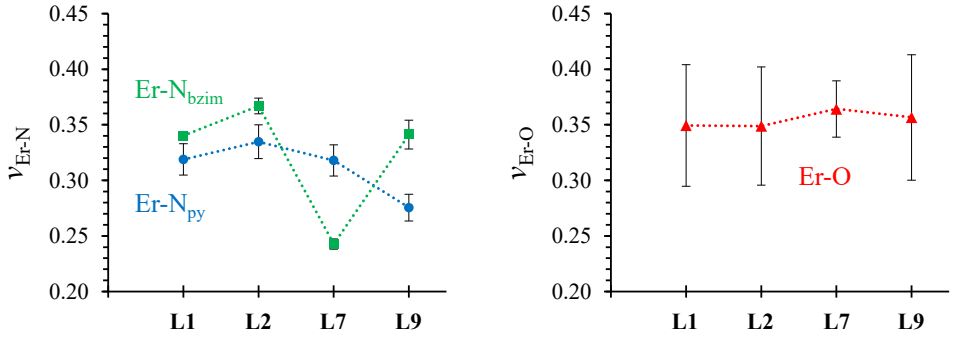

Figure 3. Average $\nu_{Er–Nbenzimidazole}$ (green), $\nu_{Er–Npyridine}$ (blue), and average $\nu_{Er–O(hfa)}$ (red) bond valences[70] calculated with eq (A1-2) for the molecular structure of complexes [**L*k***Er(hfa)$_3$] (**L*k*** = **L1**, **L2**, **L7** and **L9**) in their crystalline state. Standard deviations of the average are shown with vertical error bars. The dashed traces are only guides for the eyes.

Photophysical properties of ligands L1-L9 and of their heteroleptic complexes [L*k*Er(hfa)$_3$] in solution. The absorption spectra of the free ligands (Figures 4a, S6a, and S7a) are dominated by series of $^1\pi_i^*\leftarrow{}^1\pi$ transitions characteristic for 2,6-bis(benzimidazole)pyridine-type units.[71] For the non-conjugated ligands **L1**-**L5** and **L9**, which possess localized 10+6+10 π-electrons systems (bzim-py-bzim) according to *Clar*'s rule of aromaticity,[72],[73] the main $^1\pi^*\leftarrow{}^1\pi$ absorption band centered around 31000 cm^{-1} (Figures 4a and S6a) is split upon complexation to Er(hfa)$_3$ to give an additional lower energy band around 28000 cm^{-1} (Figures 4b and S6b), which is diagnostic for the formation of the [**L*k***Er(hfa)$_3$] adducts in solution.[66],[74] Obviously, the absorption spectra of all [**L*k***Er(hfa)$_3$] integrate the

contribution of $^1\pi^*\leftarrow{}^1\pi$ transition centered on the bound hfa$^-$ anions at 33000 cm^{-1} (identified for [**dig**Er(hfa)$_3$] with black traces in Figures 4b, S6b, and S7b). In contrast, the delocalized 30 π-electrons aromatic backbones characterizing the rigid ligands **L6-L8** extend the π-systems and result in (i) a *ca.* 1000 cm^{-1} red-shift of the main $^1\pi_2^*\leftarrow{}^1\pi$ absorption bands and (ii) the appearance of an additional vibrationally-structured $^1\pi_1^*\leftarrow{}^1\pi$ transition at lower energy (0-0 origin at 22000 cm^{-1} with 1400 cm^{-1} progression, Figures 4a and S7a).[75] Since the rigid preorganized ligands **L6-L8** retain their shape and their aromatic character upon coordination to a metallic center, the absorption spectra of the resulting [**L*k***Er(hfa)$_3$] adducts are essentially comparable with those of the pertinent unbound ligands (Figures 4 and S7). This similarity is accompanied by an apparent redshift of about 1200 cm^{-1}, which can be assigned to the Lewis acid nature of bound trivalent lanthanides.

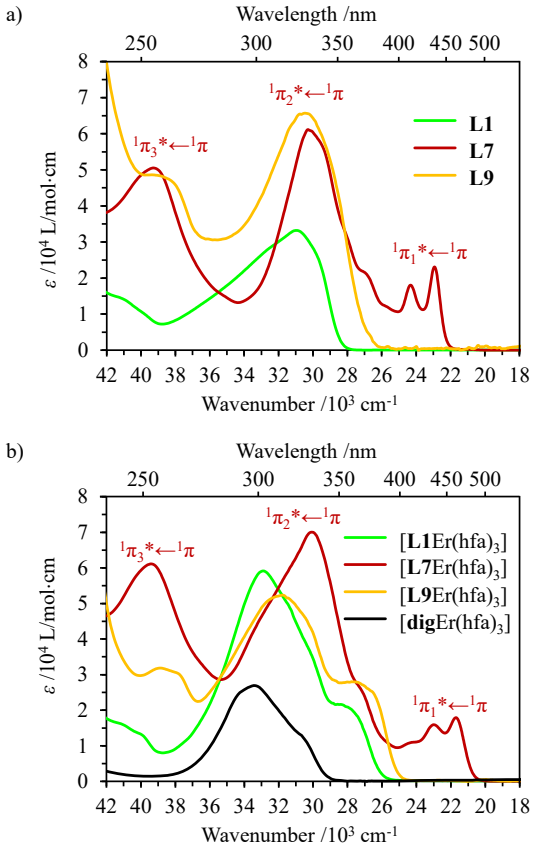

Figure 4. Selected UV-Vis absorption spectra of a) ligands **L1**, **L7** and **L9**, and b) corresponding [**L*k***Er(hfa)$_3$] and [**dig**Er(hfa)$_3$] complexes (5·10^{-6} M in CH_2Cl_2, 293 K).

At the low concentrations used, the low-intensity Laporte-forbidden f→f transitions could not be detected. Concomitant measurements using concentrated solutions (~5 mM) indeed allowed the assessment of weak Er($^{2S+1}L_J$←$^4I_{15/2}$) absorption transitions ($\varepsilon \approx 1$–80 L/mol·cm) covering the 6000–20000 cm^{-1} spectral window (Figures 5 and S8). Besides these transitions, the absorption spectra exhibited bands arising from the second and third overtones of C–H vibration frequencies around 6000 and 8500 cm^{-1}, respectively (Figure S8). A look at the Er-centered absorption spectra of [**L*k***Er(hfa)$_3$] confirms that the energies of f-f transitions are globally not affected by the nature of the tridentate heteroaromatic chromophore bound to the Er(III) center, but the contrasting change in intensity and in shape of the pseudo-hypersensitive Er($^2H_{11/2}$←$^4I_{15/2}$) transition (which mixes with the 'true' hypersentitive high-energy Er($^4G_{11/2}$←$^4I_{15/2}$) transition by spin-orbit coupling),[63],[64] does highlight some differences in going from a homoleptic D_3-symmetrical [Er(Et-bzimpy)$_3$]$^{3+}$ triple helical complex toward C_{2v}-symmetrical [**L*k***Er(hfa)$_3$] complexes (Figures 5 and S8). The latter point can be quantified by the estimation of the radiative lifetime $\tau_{rad}^{J'\to J} = 1/k_{rad}^{J'\to J}$ for each Er($^{2S+1}L_J$) excited level using the Strickler-Berg eqs (3)-(4), according that its luminescent transitions terminate onto the ground Er($^4I_{15/2}$) level (Table S10). In eq (3), $\int \varepsilon(\tilde{\nu})d\tilde{\nu}$ is the integrated spectrum of the incriminated absorption transition recorded in solution (in M^{-1}·cm^{-2}), J and J' refer to the ground (J = 15/2) and excited states, respectively, n is the refractive index of the medium, N_A is Avogadro's number (in mol^{-1}), c is the speed of light in vacuum (in cm·s^{-1}), and $\tilde{\nu}_m$ is the barycenter of the transition (in cm^{-1}) given in eq. (4).[76],[77]

$$k_{rad}^{J'\to J} = \frac{1}{\tau_{rad}^{J'\to J}} = 2303 \times \frac{8\pi c n^2 \tilde{\nu}_m{}^2 (2J+1)}{N_A (2J'+1)} \int \varepsilon(\tilde{\nu}) d\tilde{\nu} \quad (3)$$

$$\tilde{\nu}_m = \frac{\int \tilde{\nu} \cdot \varepsilon(\tilde{\nu}) d\tilde{\nu}}{\int \varepsilon(\tilde{\nu}) d\tilde{\nu}} \quad (4)$$

The experimental $\tau_{rad}^{J'\rightarrow J=15/2}$ extracted for the Er($^{2S+1}L_{J'}$) excited levels located within the 6000-20000 cm^{-1} domain cover the 0.02-13 ms range in agreement with the symmetry-forbidden character of the intrashell f-f electric dipole transitions (Figures 5 and S8). As expected from the dependence of the Einstein coefficient for spontaneous emission with $\tilde{\nu}_m$,[78] the radiative lifetimes globally decrease with increasing energy gaps (Table S10), but their abrupt drop for the pseudo-hypersensitive Er($^2H_{11/2}\leftarrow{}^4I_{15/2}$) transition reflects some extreme sensitivity of the latter transition to (i) local symmetry affecting the mixing between $4f^N$ states and the opposite parity intra-metal excitation configurations (Judd-Ofelt theory),[63] and/or mixing with intra-ligand excitation configurations (dynamic coupling).[64] In this context, one notes that the shortest radiative lifetimes $0.02 \leq \tau_{rad}(^2H_{11/2}\leftarrow{}^4I_{15/2}) \leq 0.04$ ms are obtained for [**L*k***Er(hfa)$_3$] with the extended 30 π-electrons polyaromatic ligands **L6-L8** (Table S10), which display low-energy intra-ligand excitations (Figure 4b). The latter complexes are therefore good candidates for maximizing the target green Er($^2H_{11/2}\rightarrow{}^4I_{15/2}$) and Er($^4S_{3/2}\rightarrow{}^4I_{15/2}$) (upconverted) emissions.

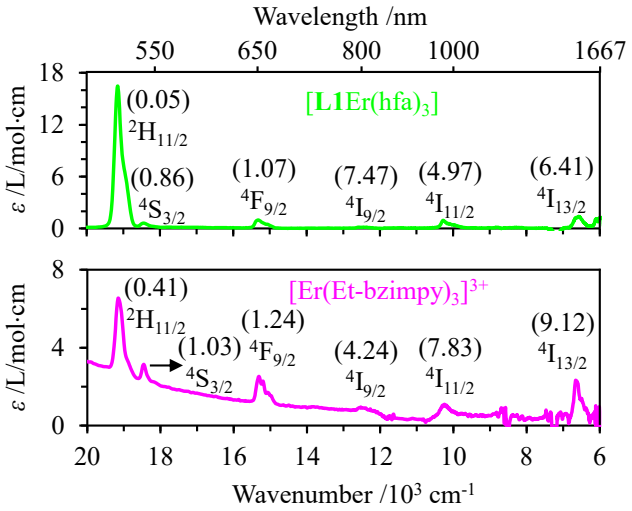

Figure 5. Visible to near-infrared absorption spectra of [**L1**Er(hfa)$_3$] (5 mM in CH_2Cl_2) and triple-stranded [Er(Et-bzimpy)$_3$]$^{3+}$ (3 mM in CH_3CN) at 293 K showing the Er($^{2S+1}L_J\leftarrow{}^4I_{15/2}$) transitions and the associated radiative lifetimes (in ms) between parentheses.

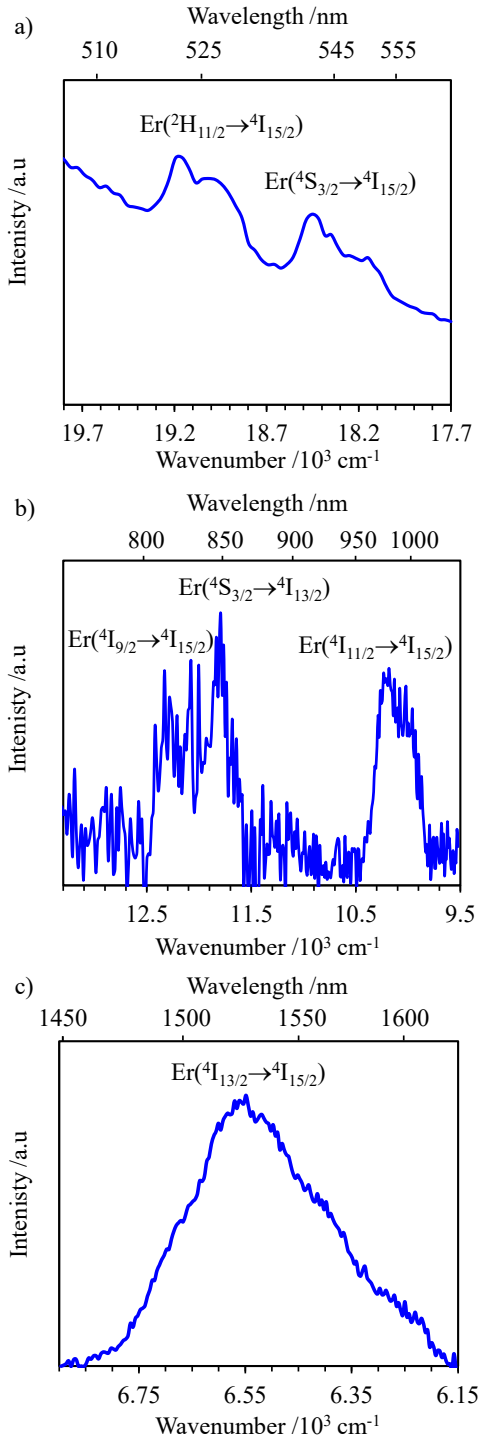

Figure 6. Emission spectra (λ_{exc} = 350 nm) recorded for [**L5**Er(hfa)$_3$] in dichloromethane solution (C ≈ 5·10^{-6} M) highlighting the spectral windows associated with Er-centered transitions at room temperature.

Excitation of [**L*k***Er(hfa)$_3$] in solution at 350 nm limits sensitization *via* the bound N-donor tridentate ligands and excludes contribution from the hfa$^-$ co-ligands. The resulting emission

spectra at 293 K show the tridentate ligand-centered singlet $^1\pi_1^* \rightarrow {}^1\pi$ emission in the UV-Vis region (Figure S9), together with minor Er-centered emission following intramolecular ligand-to-metal energy transfers (Figures S10-S12). The global 5000 cm^{-1} red-shift of the $^1\pi_1^* \rightarrow {}^1\pi$ transitions observed in going from the 'broken' 10+6+10 π-electrons polyaromatic ligands (**L1**-**L5**, **L9**, 27000-22000 cm^{-1}, Figure S9) to the extended 30 π-electrons systems (**L6**-**L8**, 23000-16000 cm^{-1}, Figure S9a) mirrors the related drift observed in the absorption spectra (Figure 4). The same conclusion holds for frozen solutions at 77 K, while some additional broad ligand-centered emission residues, assigned to $^3\pi_1^* \rightarrow {}^1\pi$ phosphorescence boosted by the heavy atom effect,[79] could be detected at lower energy for the brominated [**L4**Er(hfa)$_3$], [**L5**Er(hfa)$_3$], and [**L9**Er(hfa)$_3$] complexes (Figure S9b). In this context, the improved $^1\pi^* \rightarrow {}^3\pi^*$ intersystem crossing operating in the latter complexes favors energy transfer onto the erbium emitter which exhibits visible Er($^2H_{11/2} \rightarrow {}^4I_{15/2}$) and Er($^4S_{3/2} \rightarrow {}^4I_{15/2}$) emissions in the 500–580 nm range (Figures 6a and S10a).[80],[81] We took advantage of this improved green luminescence for the challenging determination of $\tau_{tot}^{^4S_{3/2}}$ = 3.5(2) ns, which corresponds to the total lifetime of the Er($^4S_{3/2}$) excited level in [**L4**Er(hfa)$_3$] (dichloromethane at 293 K, Table 1, column 3) by using pulsed ligand centered excitation at λ_{ex} = 355 nm followed by time-dependent detection at λ_{em} = 542 nm ($^4S_{3/2} \rightarrow {}^4I_{15/2}$). This rare experimental data updates $\tau_{tot}^{^4S_{3/2}}$ = 40 ns previously reported[82] for the triple-helical complex [GaErGa**L**$_3$](CF$_3$SO$_3$)$_9$ in the solid state at 3 K and $\tau_{tot}^{^4S_{3/2}}$ = 20(2) ns measured at 293 K for [GaErGa**L**$_3$]$^{9+}$ in acetonitrile with our novel setup. The faint associated intrinsic quantum yields $10^{-6} \leq \phi_{Er}^{^4S_{3/2}} = \tau_{tot}^{^4S_{3/2}} / \tau_{rad}^{^4S_{3/2}} \leq 5 \cdot 10^{-5}$ estimated for the [**L*k***Er(hfa)$_3$] complexes (Table 1, columns 4-5) represent a severe handicap to the implementation of efficient NIR-to-Visible (green) upconverted signals induced in erbium(III) molecular complexes in solution (eq 2).

Table 1. Radiative lifetimes (τ_{rad}) for the Er($^4S_{3/2}\rightarrow{}^4I_{15/2}$) and Er($^4I_{13/2}\rightarrow{}^4I_{15/2}$) transitions computed with eqs (3)-(4), experimental excited-state lifetimes (τ_{tot}) for the Er($^4S_{3/2}$) and Er($^4I_{13/2}$) levels and associated intrinsic quantum yields ($\phi_{Er}^{^{2S+1}L_J} = \tau_{tot}^{^{2S+1}L_J} / \tau_{rad}^{^{2S+1}L_J}$) in [**Lk**Er(hfa)$_3$] and [Er(Et-bzimpy)$_3$]$^{3+}$ in solution at 293K.

Complexes	Solvent	Er($^4S_{3/2}$) τ_{rad}/ms	Er($^4S_{3/2}$) τ_{tot}/ns	Er($^4S_{3/2}$) ϕ_{Er}[a]	Er($^4S_{3/2}$) ϕ_{Er}[b]	Er($^4I_{13/2}$) τ_{rad}/ms	Er($^4I_{13/2}$) τ_{tot}/μs	Er($^4I_{13/2}$) ϕ_{Er}
[Er(Et-bzimpy)$_3$]$^{3+}$	CH_3CN	1.31(9)	20(2)	$1.5(2)\cdot10^{-5}$	–	7.12(5)	5.57(6)	$7.8(1)\cdot10^{-4}$
[**dig**Er(hfa)$_3$]	CH_2Cl_2	0.51(2)	–	$3.9(4)\cdot10^{-5}$	$6.9(4)\cdot10^{-6}$	5.0(2)	–	–
[**L1**Er(hfa)$_3$]	CH_2Cl_2	0.89(4)	–	$2.2(2)\cdot10^{-5}$	$3.9(2)\cdot10^{-6}$	6.4(3)	2.86(3)	$4.5(2)\cdot10^{-4}$
[**L2**Er(hfa)$_3$]	CH_3CN	1.85(8)	–	$1.1(1)\cdot10^{-5}$	$1.9(1)\cdot10^{-6}$	3.5(2)	2.87(4)	$9.6(5)\cdot10^{-4}$
[**L3**Er(hfa)$_3$]	CH_2Cl_2	0.73(3)	–	$2.7(3)\cdot10^{-5}$	$4.8(3)\cdot10^{-6}$	6.6(3)	–	–
[**L4**Er(hfa)$_3$]	CH_2Cl_2	0.95(4)	3.5(2)	$2.1(2)\cdot10^{-5}$	$3.7(2)\cdot10^{-6}$	6.2(3)	2.83(3)	$4.6(2)\cdot10^{-4}$
[**L5**Er(hfa)$_3$]	CH_2Cl_2	0.96(4)	–	$2.1(2)\cdot10^{-5}$	$3.6(2)\cdot10^{-6}$	6.5(3)	2.79(3)	$4.3(2)\cdot10^{-4}$
[**L6**Er(hfa)$_3$]	CH_2Cl_2	0.32(1)	–	$6.3(7)\cdot10^{-5}$	$1.1(6)\cdot10^{-6}$	4.7(2)	3.15(3)	$6.7(3)\cdot10^{-4}$
[**L7**Er(hfa)$_3$]	CH_2Cl_2	0.64(3)	–	$3.1(3)\cdot10^{-5}$	$5.5(3)\cdot10^{-6}$	7.9(4)	3.13(5)	$3.9(2)\cdot10^{-4}$
[**L8**Er(hfa)$_3$]	CH_2Cl_2	0.69(3)	–	$2.9(3)\cdot10^{-5}$	$5.1(3)\cdot10^{-6}$	7.5(3)	3.14(3)	$4.2(2)\cdot10^{-4}$
[**L9**Er(hfa)$_3$]	CH_2Cl_2	1.10(5)	–	$1.8(2)\cdot10^{-5}$	$3.2(2)\cdot10^{-6}$	12.6(6)	2.98(3)	$2.4(1)\cdot10^{-4}$

[a]Calculated by taking τ_{tot} = 20 ns measured for the model complex [GaErGa**L**$_3$]$^{9+}$ (see main text).[82] [b]Calculated by taking τ_{tot} = 3.5 ns.

Interestingly, the red Er($^4F_{9/2}\rightarrow{}^4I_{15/2}$) emission was never observed for the [**L*k***Er(hfa)$_3$] under steady-state UV excitation, which implies that the non-radiative process from $^4S_{3/2}$ to $^4F_{9/2}$ (energy gap ≈ 3500 cm^{-1}) lacks efficiency as previously reported for erbium cations bound to other rigid multidentate polyaromatic ligands.[44],[47],[58]-[60] An ultimate look at the emission spectra of [**L*k***Er(hfa)$_3$] shows emission bands assigned to Er($^4I_J\rightarrow{}^4I_{15/2}$) electronic transitions occurring within the ground state ^{4}I atomic term (Scheme 2, Figures 6b,c and S11-S12). The associated excitation spectra (λ_{em} = 1531 nm, Figure S13) perfectly match the absorption spectra. This demonstrates that all ligand-based excited state levels contribute to the antenna effect, which eventually induces the well-known microsecond infrared Er($^4I_{13/2}\rightarrow{}^4I_{15/2}$) emission (Table 1, column 8; associated intrinsic IR quantum yields $10^{-4} \leq \phi_{Er}^{^4I_{13/2}} = \tau_{tot}^{^4I_{13/2}} / \tau_{rad}^{^4I_{13/2}} \leq 10^{-3}$, Table 1, column 9).[83],[84]

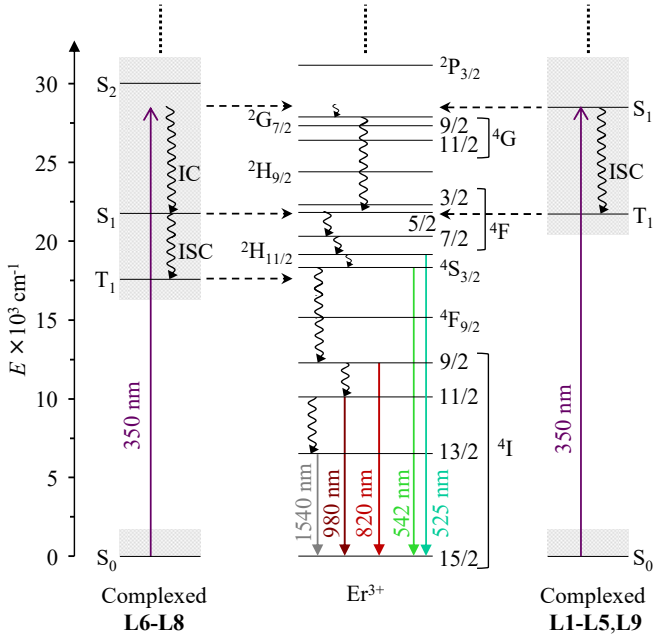

Scheme 2. Jabłoński diagram summarizing the excitation processes (straight upward arrows), energy transfers (dashed arrows), non-radiative multi-phonon relaxation (undulating arrows) and radiative emission processes (straight downward arrows) operating in the heteroleptic complexes [**L*k***Er(hfa)$_3$] (**L*k*** = **1-9**). Ligand-to-metal energy transfers arising from both singlet and triplet states are considered.

To summarize, moving from homoleptic D_3-symmetrical $[Er\mathbf{L}_3]^{3+}$ complexes (idealized D_{3h}-$[ErN_9]$ coordination environment, Figure 1)[59] to heteroleptic C_{2v}-symmetrical $[\mathbf{L}\boldsymbol{k}Er(hfa)_3]$ adducts (idealized C_{2v}-$[ErN_3O_6]$ coordination environments) maintains similar Er-based photophysical properties. However, the tunable electronic nature of the bound tridentate polyaromatic ligands **L1-L9** can be exploited to influence (i) the sensitization possibilities via π-aromatic delocalization and (ii) the final ligand-centered and erbium-centered emission output of the complexes via the control of intersystem crossing (heavy atom effect) and of intramolecular ligand-to-erbium energy transfers (phonon-assisted mechanism, Scheme 2).

Single-center NIR→VIS light upconversion in heteroleptic complexes [L*k*Er(hfa)$_3$] in solution. Having established that (i) at least one of the intermediate Er(^4I_J) excited states (J = 9/2, 11/2 or 13/2) possesses a lifetime long-enough to potentially act as emitter for downshifting, or as relay for upconversion in the heteroleptic $[\mathbf{L}\boldsymbol{k}Er(hfa)_3]$ complexes, and (ii) the Er($^2H_{11/2}$), Er($^4S_{3/2}$), and Er($^4I_{13/2}$) excited levels are luminescent, it is not so surprising that direct continuous 801 nm diode laser excitation into the Er($^4I_{9/2}$←$^4I_{15/2}$) transition (molar absorption coefficients $0.10 \leq \varepsilon_{801} \leq 0.30$ L/mol·cm, Table S11, column 2) reveals dual downshifted infrared Er($^4I_{13/2}$→$^4I_{15/2}$) emissions (1540 nm) induced by linear one-photon processes (slope n = 0.95(1)–1.02(3) for the log(I_{DS})–log(P) plots, Figures S14-S15), and challenging two-photons visible upconverted Er($^2H_{11/2}$→$^4I_{15/2}$) and Er($^4S_{3/2}$→$^4I_{15/2}$) emissions depicted in Figure 7 (slope n = 1.26(6) - 2.16(7) for the corresponding log(I_{UC})–log(P) plots, Figures S16-S17). The complete lack of residual ligand-centered $^{1,3}\pi^*\rightarrow{}^1\pi$ emission bands following NIR excitation at 801 nm (Figures 7, S14-S15) rules out the possibility for ligand-centered non-linear two-photon absorption processes.[85][86] Furthermore, at these reasonable incident power intensities (1–25 W·cm^{-2}), there is no realistic option for the operation of competitive non-linear Er-centered processes.[87],[88]

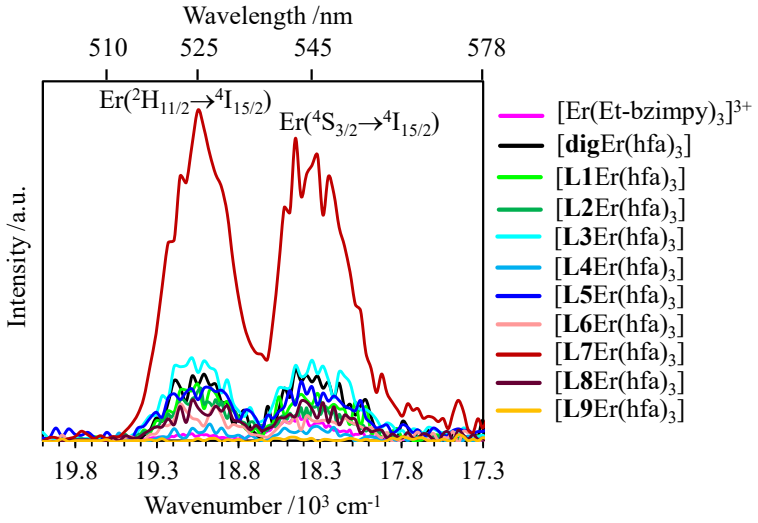

Figure 7. Upconverted visible Er($^2H_{11/2}\rightarrow{}^4I_{15/2}$) and Er($^4S_{3/2}\rightarrow{}^4I_{15/2}$) emissions observed for [**L*k***Er(hfa)$_3$] complexes recorded upon laser excitation of the Er($^4I_{9/2}\leftarrow{}^4I_{15/2}$) transition at λ_{exc} = 801 nm ($\tilde{\nu}_{exc}$ = 12284 cm^{-1}) and using incident pump intensity P = 14.3 W·cm^{-2} in dichloromethane solution (5 mM) at 293K (measurements for [**L2**Er(hfa)$_3$] and [Er(Et-bzimpy)$_3$]$^{3+}$ complexes were performed in CH_3CN under the same conditions).

Quantitative data for the upconversion processes are based on the upconversion quantum yields ϕ_{tot}^{up} (Figure 8 and Table S11, column 6) obtained by laser excitation of [**L*k***Er(hfa)$_3$] at λ_{exc} = 801 nm with incident pump intensity of 1 W focused on a spot size of ≈ 0.07 cm^2 in dichloromethane solutions[59] and using indocyanine green (ICG) as the standard (λ_{exc} = 801 nm, P = 5 mW focused on a spot size of ≈ 0.07 cm^2, Φ_s = 0.132 in ethanol at 293K,[89] see Appendix 1 for details). The trend in the upconversion quantum yields (Figure 8) mirrors the upconverted intensities (Figure 7), and one immediately notes that going from the homoleptic D_3-symmetrical complex [Er(Et-bzimpy)$_3$]$^{3+}$ (ϕ_{tot}^{up} = 1.7(2)·10^{-9} normalized at 25 W·cm^{-2})[59] to the flexible heteroleptic C_{2v}-symmetrical [**L*k***Er(hfa)$_3$] adducts (**L*k*** = **L1**-**L5** and **L9**) results in a gain in upconversion quantum yield by roughly one to two orders of magnitude (1.6(2)·10^{-8} ≤ ϕ_{tot}^{up} ≤ 3.0(3)·10^{-7} normalized at 25 W·cm^{-2}). The simultaneous extension of the delocalized π-aromatic system and rigidity in the preorganized [**L*k***Er(hfa)$_3$] complexes (**L*k*** = **L6**-**L8**) further

boosts the upconversion quantum yield, which culminates at ϕ_{tot}^{up} = 1.0(1)·10^{-6} for [**L7**Er(hfa)$_3$] (normalized at 25 W·cm^{-2}, Figure 8). The latter value compares well with the best reproducible molecular-based upconversion quantum yield of ϕ_{tot}^{up} = 9(1)·10^{-7} (normalized at 25 W·cm^{-2}) reported for a doped single-emitter TbYb$_9$ hetero-nonanuclear cluster obeying the multicenter cooperative upconversion (CU) mechanism upon 980 nm excitation in CD_3OD.[54]

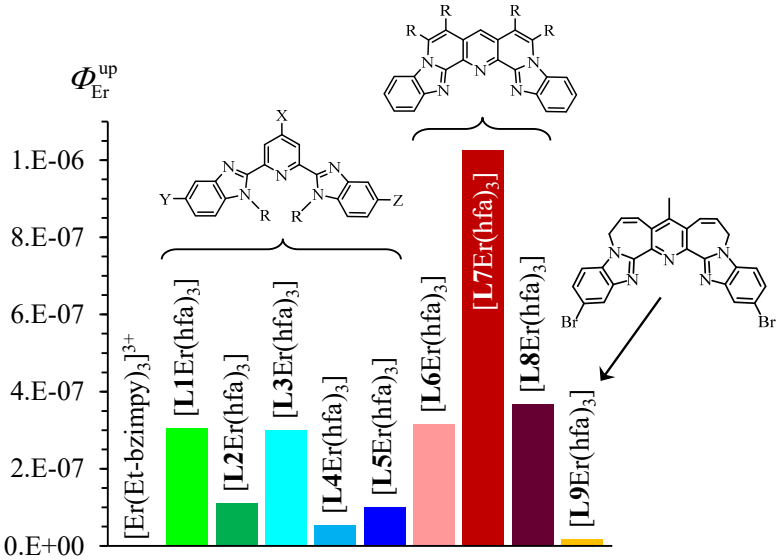

Figure 8. Upconversion luminescent quantum yields (Φ^{UC}) calculated for single-centered mononuclear complexes [**L*k***Er(hfa)$_3$] upon laser excitation of the Er($^4I_{9/2}$←$^4I_{15/2}$) transition at λ_{exc} = 801 nm ($\tilde{\nu}_{exc}$ = 12284 cm^{-1}) at 293 K normalized to P = 25 W·cm^{-2} for comparison purpose. All samples were measured in dichloromethane solutions (C ~ 5 mM) with respect to indocyanine green in ethanol, except for [Er(Et-bzimpy)$_3$]$^{3+}$ [59] and [**L2**Er(hfa)$_3$], which were measured in acetonitrile solutions (C ~ 10 mM).

Considering the minor intrinsic Er($^4S_{3/2}$) quantum yield ($10^{-6} \leq \phi_{Er}^{^4S_{3/2}} = \tau_{tot}^{^4S_{3/2}} / \tau_{rad}^{^4S_{3/2}} \leq 5 \cdot 10^{-5}$, Table 1, column 5) provides reasonable ESA efficiencies $5 \cdot 10^{-3} \leq \eta_{ESA} = \phi_{tot}^{up} / \phi_{Er}^{^4S_{3/2}} \leq 2 \cdot 10^{-1}$ for [**L*k***Er(hfa)$_3$] in solution (normalized at P = 25 W·cm^{-2}, Table S11, column 7), which overpass by two orders of magnitude η_{ESA} = 1.1(2)·10^{-4} previously reported for the homoleptic [Er(Et-bzimpy)$_3$]$^{3+}$ complex.[59] A straightforward reorganization of eq (2), which stands for the three-

level kinetic model of the ESA mechanism (Scheme 1), correlates η_{ESA} with the second excitation process characterized by its decadic molar absorption coefficient $\varepsilon_{Er}^{1\to2}$ (eq 5).

$$\eta_{Er,ESA} = \frac{\phi_{Er}^{up}}{\phi_{Er}^{^4S_{3/2}}} = \frac{k_{Er}^{exc(1\to2)}}{k_{Er}^{1\to0}} = \left(3.8\cdot10^{-21}\,\frac{\lambda_P}{hc}\,P\varepsilon_{Er}^{1\to2}\right)\tau_{Er}^{|1\rangle} \qquad (5)$$

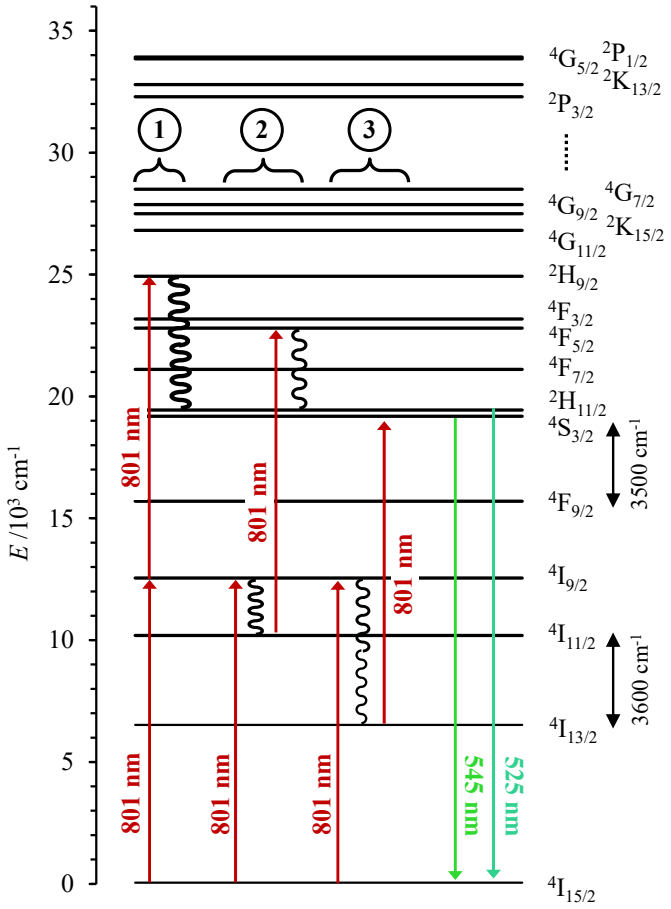

Scheme 3. Jabłoński diagram summarizing the possible mechanisms (1-3) of the Er-centered upconversion processes operating in the complexes [**L*k***Er(hfa)$_3$] upon excitation of the Er(^{4}I$_{9/2}$←^{4}I$_{15/2}$) transition at 801 nm. Excitation (upward arrows), non-radiative multiphonon relaxation (undulating arrows) and emission (downward arrows). The energies of the level are taken for the free ions.[90]

First considering the ESA mechanism (3) in Scheme 3, in which Er(^{4}I$_{13/2}$) works as the long-lived excited relay (microsecond range, Table 1, column 8) returns $4\cdot10^3 \le \varepsilon_{Er}^{1\to2} \le 5\cdot10^5$ L/mol·cm with eq (5) for the second absorption event (Table S11, column 8). These huge

absorption coefficients are out of the accessible range theoretically computed for the incriminated $^4S_{3/2}\leftarrow{}^4I_{13/2}$ second excitation,[59] and, more generally, for any internal 4f→4f transitions (1-500 L/mol·cm).[63] We conclude that the microsecond luminescent Er($^4I_{13/2}$) level does not contribute significantly as a relay for the erbium-based ESA upconversion in these complexes (ESA mechanism ③ in Scheme 3), a claim further confirmed by the lack of correlation between $\eta_{Er,ESA}$ and $\tau_{Er}^{|^4I_{13/2}\rangle}$ (Figure S18) despite the theoretical link predicted in eq (5). Alternatively, the Er($^4I_{11/2}$) level (ESA mechanism ② in Scheme 3) and/or Er($^4I_{9/2}$) level (ESA mechanism ① in Scheme 3) in [**L*k***Er(hfa)$_3$] should be considered as potential long-lived relays. This is supported by the detection of Er($^4I_{11/2}\rightarrow{}^4I_{15/2}$) and Er($^4I_{9/2}\rightarrow{}^4I_{15/2}$) radiative emission upon ligand-based excitation (Figures 6b and S11) despite their long radiative lifetimes (4-12 ms, Table S10), which usually prevent their detection in molecules possessing high-energy vibrations and thus efficient non-radiative relaxation pathways. Although the latter emission intensities were too weak to record reliable experimental lifetimes for the Er($^4I_{11/2}$) and Er($^4I_{9/2}$) levels in these complexes with our setup, one notices that the incriminated energy gap ΔE = 3600 cm^{-1} separating the Er($^4I_{11/2}$) and Er($^4I_{13/2}$) levels, fairly matches the related 3500 cm^{-1} energy separation between Er($^4S_{3/2}$) to Er($^4F_{9/2}$) levels in [**L*k***Er(hfa)$_3$] (Scheme 3, right).[90] The lack of efficient phonon bath in this energy range, which prevents the observation of red Er($^4F_{9/2}\rightarrow{}^4I_{15/2}$) emission in these complexes,[60] may similarly drastically limit non-radiative Er($^4I_{11/2}$) to Er($^4I_{13/2}$) relaxation with the consequent existence of long-lived Er($^4I_{11/2}$) excited relays and the operation of an efficient ESA mechanism ② depicted in Scheme 3.[91] With this in mind, it is probably worth stressing here that the largest upconversion quantum yield of ϕ_{tot}^{up} = 1.0(1)·10^{-6} is observed for [**L7**Er(hfa)$_3$] (normalized at 25 W·cm^{-2}, Figure 8), being the only complex devoid of high-energy C-H$_{aliphatique}$ stretching vibrations around 3000 cm^{-1} (Figure S5). This suggests that overlap between the putative Er($^4I_{11/2}\rightarrow{}^4I_{13/2}$) emission and the vibrational

absorption cross section of the CH quenchers in this energy range plays a crucial role. The intense CH_3-stretching vibrations measured in the 3000 cm^{-1} range for the [**L*k***Er(hfa)$_3$] adducts possessing alkyl groups should therefore contribute more efficiently to the non-radiative relaxation of the Er($^4I_{11/2}$) relay compared with the much weaker aromatic CH vibrations (Figure S5).

Conclusion

Moving from idealized D_{3h}-symmetrical triple-helical [ErN_9] chromophores, found in [Er(Et-bimpy)$_3$]$^{3+}$ (Figure 1), toward idealized C_{2v}-[ErN_3O_6] units in C_{2v}-symmetrical [**L*k***Er(hfa)$_3$] adducts (Figure 2) boosts the efficiency of the ESA upconversion mechanism by 2-3 orders of magnitude (Figure 8), which makes molecular-based ESA a concurrent to multicenter ETU and CU processes. Detailed photophysical studies strongly suggest that the origin of this remarkable effect finds its root in the existence of a long-lived Er($^4I_{11/2}$) level resulting from the specific lack of efficient relaxation processes in the 3500 cm^{-1} range accompanying the concomitant binding of perfluorinated hfa^- co-ligands and rigid polyaromatic **L*k*** guests to Er(III) in [**L*k***Er(hfa)$_3$]. An ultimate proof for the dominance of mechanism ② operating in these mononuclear complexes is currently under investigation with the technical development of ultra-sensitive time-gated NIR detection following intense pulsed NIR excitation of Er($^4I_{9/2}\leftarrow{}^4I_{15/2}$) at 801 nm and of Er($^4I_{11/2}\leftarrow{}^4I_{15/2}$) at 966 nm.

Acknowledgements

This work is supported from the Swiss National Science Foundation (grant 200020_207313).

Conflict of Interest

The authors declared no conflict of interest.

Data Availability Statement

The data that support the findings of this study are available from the corresponding authors upon reasonable request.

Keywords: molecular upconversion, erbium, heteroleptic complexes, single molecule.

References

[1] P. N. Prasad, D. J. Williams, *Introduction to Nonlinear Optical Effects in Molecules & Polymers*, John Wiley & Sons, Inc., New York – Chichester – Brisbane -Toronto – Singapore, 1991.

[2] M. Goeppert-Mayer, *Ann. Phys.* **1931**, *9*, 273-294.

[3] J. Kerr, *Philos. Mag. Ser. 4* **1875**, *50*, 337–348.

[4] J. Kerr, *Philos. Mag. Ser. 4* **1875**, *50*, 446–458.

[5] G. S. He, L.-S. Tan, Q. Zheng, P. N. Prasad, *Chem. Rev.* **2008**, *108*, 1245-1330.

[6] R. Medishetty, J. K. Zareba, D. Mayer, M. Samoc, R. A. Fischer, *Chem. Soc. Rev.* **2017**, *46*, 4976-5004.

[7] T. H. Maiman, *Nature* **1960**, *187*, 493-494.

[8] P. A. Franken, G. Weinreich, C. W. Peters, A. E. Hill, *Phys. Rev. Lett.* **1961**, *7*, 118.

[9] W. Kaiser, C. G. B. Garrett, *Phys. Rev. Lett.* **1961**, *7*, 229.

[10] P. Neveu, I. Aujard, C. Benbrahim, T. Le Saux, J.-F. Allemand, S. Vriz, D. Bensimon, L. Jullien, *Angew. Chem. Int. Ed.* **2008**, *47*, 3744-3746.

[11] D. K. Sinha, P. Neveu, N. Gagey, I. Aujard, C. Benbrahim-Bouzidi, T. Le Saux, C. Rampon, C. Gauron, B. Goetz, S. Dubruille, M. Baaden, M. Volovitch, D, Bensimon, S. Vriz, L. Jullien, *Chembiochem.* **2010**, *11*, 653-663.

[12] A. D'Aléo, C. Andraud, O. Maury, *Luminescence of Lanthanide Ions in Coordination Compounds and Nanomaterials*, A. de Bettencourt-Dias (Ed.), Wiley, Chichester, 2014, chap 5, 197-230.

[13] A. T.Bui, M. Beyler, A. Grichine, A. Duperray, J.-C. Mulatier, Y. Guyot, C. Andraud, R. Tripier, S. Brasselet, O. Maury, *Chem. Commun.* **2017**, *53*, 6005-6008.

[14] T. N. Nguyen, F. M. Ebrahim, K. C. Stylianou, *Coord. Chem. Rev.* **2018**, *377*, 259-306.

[15] S. Pascal, S. David, C. Andraud O. Maury, *Chem. Soc. Rev.* **2021**, *50*, 6613-6658.

[16] S. David, H. J. Chang, C. Lopes, C. Brannlund, B. Le Guennic, C. Berginc, E. Van Stryland, M. V. Bondar, D. Hagan, D. Jacquemin, C. Andraud, O. Maury, *Chem. Eur. J.* **2021**, *27*, 3517-3525.

[17] F. Auzel, *J. Lumin.* **2020**, *223*, 116900.

[18] H. Bolvin, A. Furstenberg, B. Golesorkhi, H. Nozary, I. Taarit, C. Piguet, *Acc. Chem. Res.* **2022**, *55*, 442-456.

[19] N. Bloembergen, *Phys. Rev. Lett.* **1959**, *2*, 84-85.

[20] C. A. Parker, C. G. Hatchard, *Proc. Chem. Soc.* **1962**, 386-387.

[21] C. A. Parker, C. G. Hatchard, *Proc. Chem. Soc. A* **1962**, *269*, 574-584.

[22] J. F. Porter, *Phys. Rev. Lett.* **1961**, *7*, 414-415.

[23] F. Auzel, *C. R. Acad. Sc. Paris* **1966**, *B263*, 819-821.

[24] T. W. Schmidt, F. N. Castellano, *J. Phys. Chem. Lett.* **2014**, *5*, 4062-4072.

[25] J. Zhou, Q. Liu, W. Feng, Y. Sun, F. Li, *Chem. Rev.* **2015**, *115*, 395-465.

[26] P. Bharmoria, H. Bildirir, K. Moth-Poulsen, *Chem. Soc. Rev.* **2020**, *49*, 6529-6554.

[27] F. Edhborg, H. Bildirir, P. Bharmoria, K. Moth-Poulsen, B. Albinsson, *J. Phys. Chem. B* **2021**, *125*, 6255-6263.

[28] V. Gray, D. Dzebo, M. Abrahamsson, B. Albinsson, K. Moth-Poulsen, *Phys. Chem. Chem. Phys.* **2014**, *16*, 10345-10352.

[29] B. S. Richards, D. Hudry, D. Busko, A. Turshatov, I. A. Howard, *Chem. Rev.* **2021**, *121*, 9165-9195.

[30] S. Y. Han, R. R. Deng, Q. F. Gu, L. M. Ni, U. Huynh, J. B. Zhang, Z. G. Yi, B. D. Zhao, H. Tamura, A. Pershin, H. Xu, Z. Y. Huang, S. Ahmad, M. Abdi-Jalebi, A. Sadhanala, M. L. Tang, A. Bakulin, D. Beljonne, X. G. Liu, A. Rao, *Nature* **2020**, *587*, 594-599.

[31] F. Auzel, *C. R. Acad. Sc. Paris* **1966**, *B262*, 1016-1019.

[32] F. Auzel, *Chem. Rev.* **2004**, *104*, 139-173.

[33] S. Han, R. Deng, X. Liu, *Angew. Chem. Int. Ed.* **2014**, *53*, 11702-11715.

[34] D. M. Wu, A. Garcia-Etxarri, A. Salleo, J. A. Dionne, *J. Phys. Chem. Lett.* **2014**, *5*, 4020-4031.

[35] S. B. Liu, L. Yan, J. S. Huang, Q. Y. Zhang, B. Zhou, *Chem. Soc. Rev.* **2022**, *51*, 1729-1765.

[36] X.-Y. Wang, R. R. Valiev, T. Y. Ohulchanskyy, H. Agren, C. Yang, G. Chen, *Chem. Soc. Rev.* **2017**, *46*, 4150-4167.

[37] G. C. Bao, S. H. Wen, G. G. Lin, J. L. Yuan, J. Lin, K. L. Wong, J. C. G. Bünzli, D. Y. Jin, *Coord. Chem. Rev.* **2021**, *429*, 213642.

[38] R. Martin-Rodriguez, S. Fischer, A. Ivaturi, B. Froehlich, K. W. Krämer, J. C. Goldschmidt, B. S. Richards, A. Meijerink, *Chem. Mater.* **2013**, *25*, 1912-1921.

[39] M. Kaiser, C. Wurth, M. Kraft, I. Hyppanen, T. Soukka, U. Resch-Genger, *Nanoscale* **2017**, *9*, 10051-10058.

[40] M. S. Meijer, P. A. Rojas-Gutierrez, D. Busko, I. A. Howard, F. Frenze, C. Wurth, U. Resch-Genger, B. S. Richards, A. Turshatov, J. A. Capobianco, S. Bonnet, *Phys. Chem. Chem. Phys.* **2018**, *20*, 22556-22562.

[41] C. Reinhard, H. U. Güdel, *Inorg. Chem.* **2002**, *41*, 1048-1055.

[42] L. Aboshyan-Sorgho, C. Besnard, P. Pattison, K. R. Kittilstved, A. Aebischer, J.-C. G. Bünzli, A. Hauser, C. Piguet, *Angew. Chem. Int. Ed.* **2011**, *50*, 4108-4112.

[43] L. Aboshyan-Sorgho, M. Cantuel, S. Petoud, A. Hauser, C. Piguet, *Coord. Chem. Rev.* **2012**, *256*, 1644-1663.

[44] Y. Suffren, B. Golesorkhi, D. Zare, L. Guénée, H. Nozary, S. V. Eliseeva, S. Petoud, A. Hauser, C. Piguet, *Inorg. Chem.* **2016**, *55*, 9964-9972.

[45] L. J. Charbonnière, *Dalton Trans.* **2018**, *47*, 8566-8570.

[46] A. M. Nonat, L. J. Charbonnière, *Coord. Chem. Rev.* **2020**, *409*, 213192.

[47] B. Golesorkhi, H. Nozary, A. Fürstenberg, C. Piguet, *Mater. Horiz.* **2020**, *7*, 1279-1296.

[48] D. A. Galico, C. M. S. Calado, M. Murugesu, *Chem. Sci.* **2023**, *14*, 5827-5841.

[49] H. J. Yin, Z. G. Xiao, Y. S. Feng, C. J. Yao, *Materials* **2023**, *16*, 5642.

[50] J. Wang, Y. Jiang, J. Y. Liu, H. B. Xu, Y. X. Zhang, X. Peng, M. Kurmoo, S. W. Ng, M. Zeng, *Angew. Chem. Int. Ed.* **2021**, *60*, 22368-22375.

[51] B. Golesorkhi, S. Naseri, L. Guenee, I. Taarit, F. Alves, H. Nozary, C. Piguet, *J. Am. Chem. Soc.* **2021**, *143*, 15326-15334.

[52] I. Taarit, F. Alves, A. Benchohra, L. Guenee, B. Golesorkhi, A. Rosspeintner, A. Furstenberg, C. Piguet, *J. Am. Chem. Soc.* **2023**, *145*, 8621−8633.

[53] D. A. Galico, M. Murugesu, *Angew. Chem. Int. Ed.* **2022**, *61*, e202204839

[54] R. C. Knighton, L. K. Soro, L. Frances-Soriano, A. Rodriguez-Rodriguez, G. Pilet, M. Lenertz, C. Platas-Iglesias, N. Hildebrandt, L. J. Charbonnière, *Angew. Chem. Int. Ed.* **2022**, *61*, e202113114.

[55] R. C. Knighton, L. K. Soro, W. Thor, J. M. Strub, S. Cianferani, Y. Mely, M. Lenertz, K. L. Wong, C. Platas-Iglesias, F. Przybilla, L. J. Charbonnière, *J. Am. Chem. Soc.* **2022**, *144*, 13356-13365.

[56] L. K. Soro, R. C. Knighton, F. Avecilla, W. Thor, F. Przybilla, O. Jeannin, D. Esteban-Gomez, C. Platas-Iglesias, L. J. Charbonnière, *Adv. Opt. Mater.* **2022**, 2202307.

[57] B. Golesorkhi, H. Nozary, L. Guénée, A. Fürstenberg, C. Piguet, *Angew. Chem. Int. Ed.* **2018**, *57*, 15172-15176.

[58] B. Golesorkhi, A. Fürstenberg, H. Nozary, C. Piguet, *Chem. Sci.* **2019**, *10*, 6876-6885.

[59] B. Golesorkhi, I. Taarit, H. Bolvin, H. Nozary, J. R. Jimenez, C. Besnard, L. Guenee, A. Furstenberg, C. Piguet, *Dalton Trans.* **2021**, *50*, 7955-7968.

[60] Y. Gil, R. C. de Santana, A. S. S. de Camargo, L. G. Merizio, P. F. Carreno, P. Fuentealba, J. Manzur, E. Spodine, *Dalton Trans.* **2023**, *52*, 3158-3168.

[61] M. Pollnau, D. R. Gamelin, S. R. Lüthi, H.U. Güdel, *Phys. Rev.* **2000**, *B61*, 3337-3346.

[62] T. W. Schmidt, F. N. Castellano, *J. Phys. Chem. Lett.* **2014**, *5*, 4062-4072.

[63] Görller-Walrand, K. Binnemans, in *Handbook on the Physics and Chemistry of Rare Earths*, Vol. 25 (Eds.: K. A. Gschneidner, L. Eyring), Elsevier Science, Amsterdam, 1998, pp. 101-264.

[64] M. Hatanaka, S. Yabushita, *Theor. Chem. Acc.* **2014**, *133*, 1517.

[65] W. J. Evans, D. G. Giarikos, M. A. Johnston, M. A. Greci, J. W. Ziller, *J. Chem. Soc. Dalton* **2002**, 520-526.

[66] M. Mirzakhani, H. Nozary, S. Naseri, C. Besnard, L. Guénée, C. Piguet, *Inorg. Chem.* **2021**, *60*, 15529-15542.

[67] S. Naseri, M. Mirzakhani, C. Besnard, L. Guenee, L. Briant, H. Nozary, C. Piguet, *Chem. Eur. J.* **2023**, *29*, e202202727.

[68] G. Le-Hoang, L. Guénée, S. Naseri, C. Besnard, C. Piguet, *Helv. Chim. Acta* **2023**, *106*, e202200190.

[69] B. Golesorkhi, L. Guénée, H. Nozary, A. Fürstenberg, Y. Suffren, S. V. Eliseeva, S. Petoud, A. Hauser, C. Piguet, *Chem. Eur. J.* **2018**, *24*, 13158-13169.

[70] I. D. Brown, *Chem. Rev.* **2009**, *109*, 6858-6919.

[71] C. Piguet, J.-C. G. Bünzli, G. Bernardinelli, C. G. Bochet, P. Froidevaux, *J. Chem. Soc., Dalton Trans.* **1995**, 83-97.

[72] E. Clar, *The Aromatic Sextet*, John Wiley & Sons Ltd., London, New York, Sydney, Toronto 1972.

[73] M. Sola, *Front. Chem.* **2013**, *1*, ARTN 22.

[74] A. Zaïm, H. Nozary, L. Guénée, C. Besnard, J.-F. Lemonnier, S. Petoud, C. Piguet, *Chem. Eur. J.* **2012**, *18*, 7155-7168.

[75] M. Solà, A. I. Boldyrev, M. K. Cryanski, T. M. Krygowski, G. Merino, *Aromaticity and Antiaromaticity*: *Concepts and Applications.* John Wiley & Sons Ltd., Chichester, chap 8.

[76] S. J. Strickler, R. A. Berg, *J. Chem. Phys.* **1962**, *37*, 814-822.

[77] J.-C. G. Bünzli, A.-S. Chauvin, H. K. Kim, E. Deiters, S. V. Eliseeva, *Coord. Chem. Rev.* **2010**, *254*, 2623-2633.

[78] R. C. Hilborn, *Am. J. Phys.* **1982**, *50*, 982-986.

[79] T. Itoh, *Chem. Rev.* **2012**, *112*, 4541-4568.

[80] N. Sabbatini, M. Guardigli, I. Manet, in *Handbook on the Physics and Chemistry of Rare Earths*, Vol. 23 (Eds.: K. A. Gschneidner, L. Eyring), Elsevier Science, Amsterdam, **1996**, pp. 69-120.

[81] E. G. Moore, A. P. S. Samuel, K. N. Raymond, *Acc. Chem. Res.* **2009**, *42*, 542-552.

[82] Y. Suffren, D. Zare, S. V. Eliseeva, L. Guénée, H. Nozary, T. Lathion, L. Aboshyan-Sorgho, S. Petoud, A. Hauser, C. Piguet, *J. Phys. Chem. C* **2013**, *117*, 26957-26963.

[83] F. Artizzu, M. L. Mercuri, A. Serpe, P. Deplano, *Coord. Chem. Rev.* **2011**, *255*, 2514-2529.

[84] Y. Ning, M. Zhu, J.-L. Zhang, *Coord. Chem. Rev.* **2019**, *399*, 213028.

[85] R. Medishetty, J. K. Zareba, D. Mayer, M. Samoc, R. A. Fischer, *Chem. Soc. Rev.* **2017**, *46*, 4976-5004.

[86] C. Andraud, O. Maury, *Eur. J. Inorg. Chem.* **2009**, 4357–4371.

[87] T. J. Sorensen, O. A. Blackburn, M. Tropiano, S. Faulkner, *Chem. Phys. Lett.* **2012**, *541*, 16–20.

[88] O. A. Blackburn, M. Tropiano, T. J. Sorensen, J. Thom, A. Beeby, L. M. Bushby, D. Parker, L. S. Natrajan, S. Faulkner, *Phys. Chem. Chem. Phys.* **2012**, *14*, 13378–13384.

[89] K. Rurack, M. Spieles, *Anal. Chem.* **2011**, *83*, 1232–1242.

[90] M. G. Brik, C.-G. Ma, *Theoretical Spectroscopy of Transition Metal and Earth Ions: From free State to Crystal Field,* Jenny Stanford Publishing Pte. Ltd., 2020, 237-239.

[91] A. Ferrier, M. Velazquez, J. L. Doualan, R. Moncorge, *J. Opt. Soc. Am. B* **2007**, *24*, 2526-2536.

Graphical content entry:

Moving from homoleptic triple helical erbium complexes to heteroleptic adducts boosts the quantum yield of near-infrared to visible (green) molecular-based light-upconversion by three orders of magnitude in solution at room temperature.